

## Article

# Crystallization Mechanism and Optical Properties of Antimony-Germanate-Silicate Glass-Ceramic Doped with Europium Ions

Piotr Golonko <sup>1</sup>, Karolina Sadowska <sup>1</sup>, Tomasz Ragiń <sup>1</sup>, Marcin Kochanowicz <sup>1</sup>, Piotr Miluski <sup>1</sup>, Jan Dorosz <sup>1</sup>, Marta Kuwik <sup>2</sup>, Wojciech Pisarski <sup>2</sup>, Joanna Pisarska <sup>2</sup>, Magdalena Leśniak <sup>3</sup>, Dominik Dorosz <sup>3</sup> and Jacek Żmojda <sup>1,\*</sup>

- <sup>1</sup> Faculty of Electrical Engineering, Bialystok University of Technology, 45D Wiejska Street, 15-351 Bialystok, Poland; p.golonko@doktoranci.pb.edu.pl (P.G.); k.sadowska@doktoranci.pb.edu.pl (K.S.); tomasz.ragin@pb.edu.pl (T.R.); m.kochanowicz@pb.edu.pl (M.K.); p.miluski@pb.edu.pl (P.M.); doroszjan@pb.edu.pl (J.D.)
- <sup>2</sup> Institute of Chemistry, University of Silesia, 9 Szkolna Street, 40-007 Katowice, Poland; marta.kuwik88@gmail.com (M.K.); wojciech.pisarski@us.edu.pl (W.P.); joanna.pisarska@us.edu.pl (J.P.)
- <sup>3</sup> Faculty of Materials Science and Ceramics, AGH University of Science and Technology, 30 Mickiewicza Av., 30-059 Krakow, Poland; mlesniak@agh.edu.pl (M.L.); ddorosz@agh.edu.pl (D.D.)
- \* Correspondence: j.zmojda@pb.edu.pl



**Citation:** Golonko, P.; Sadowska, K.; Ragiń, T.; Kochanowicz, M.; Miluski, P.; Dorosz, J.; Kuwik, M.; Pisarski, W.; Pisarska, J.; Leśniak, M.; et al. Crystallization Mechanism and Optical Properties of Antimony-Germanate-Silicate Glass-Ceramic Doped with Europium Ions. *Materials* **2022**, *15*, 3797. <https://doi.org/10.3390/ma15113797>

Academic Editor: Nicolas Sbirrazzuoli

Received: 4 May 2022

Accepted: 24 May 2022

Published: 26 May 2022

**Publisher's Note:** MDPI stays neutral with regard to jurisdictional claims in published maps and institutional affiliations.



**Copyright:** © 2022 by the authors. Licensee MDPI, Basel, Switzerland. This article is an open access article distributed under the terms and conditions of the Creative Commons Attribution (CC BY) license (<https://creativecommons.org/licenses/by/4.0/>).

**Abstract:** Glass-ceramic is semi-novel material with many applications, but it is still problematic in obtaining fibers. This paper aims to develop a new glass-ceramic material that is a compromise between crystallization, thermal stability, and optical properties required for optical fiber technology. This compromise is made possible by an alternative method with a controlled crystallization process and a suitable choice of the chemical composition of the core material. In this way, the annealing process is eliminated, and the core material adopts a glass-ceramic character with high transparency directly in the drawing process. In the experiment, low phonon antimony-germanate-silicate glass (SGS) doped with  $\text{Eu}^{3+}$  ions and different concentrations of  $\text{P}_2\text{O}_5$  were fabricated. The glass material crystallized during the cooling process under conditions similar to the drawing processes'. Thermal stability (DSC), X-ray photo analysis (XRD), and spectroscopic were measured.  $\text{Eu}^{3+}$  ions were used as spectral probes to determine the effect of  $\text{P}_2\text{O}_5$  on the asymmetry ratio for the selected transitions ( $^5\text{D}_0 \rightarrow ^7\text{F}_1$  and  $^5\text{D}_0 \rightarrow ^7\text{F}_2$ ). From the measurements, it was observed that the material produced exhibited amorphous or glass-ceramic properties, strongly dependent on the nucleator concentration. In addition, the conducted study confirmed that europium ions co-form the  $\text{EuPO}_4$  structure during the cooling process from 730 °C to room temperature. Moreover, the asymmetry ratio was changed from over 4 to under 1. The result obtained confirms that the developed material has properties typical of transparent glass-ceramic while maintaining high thermal stability, which will enable the fabrication of fibers with the glass-ceramic core.

**Keywords:** active glass-ceramic; luminescent properties; nucleation; precursor of crystallization; antimony-germanate glass;  $\text{Eu}^{3+}$  ions; asymmetry ratio

## 1. Introduction

Glass-ceramics (GC) is a compound material with multiple application possibilities. After doping with trivalent lanthanide ions, it becomes an active glass-ceramic with many optoelectronic applications such as temperature sensing, lasers, and source of NIR, MIR, LED, displays, biomedical, and many others [1–9]. However, GC is usually used in bulk due to the technology gap in processing fibers. The lack of fiber manufacturing technology limits the application of active GCs in optical fibers; thus, the enormous potential for quantum efficiency, luminescence shaping, and other unique properties is mainly untapped [2,10,11].

Existing processing methods for glass-ceramic core optical fibers are complicated and make it impossible to obtain GC-core with a crystallization effect during the drawing process. The research in this paper leads to core materials that can crystallize during the drawing process without additional steps such as heat treatment. Rare earth (RE) ions also can be used as a spectral probe to detect structural changes [12,13]. The most used lanthanide in this role is the  $\text{Eu}^{3+}$  ion, which is used as a spectral probe to find the crystal phase of nanocomposite materials. According to the asymmetry ratio connected with  $5\text{D}_0 \rightarrow 7\text{F}_1$  and  $5\text{D}_0 \rightarrow 7\text{F}_2$  transitions, some structural changes in the vicinity of europium ions can be analyzed. The  $5\text{D}_0 \rightarrow 7\text{F}_1$  transition is essentially independent of the structure of the matter around the europium ions and can be taken as a reference point in luminescence changes. In contrast, the  $5\text{D}_0 \rightarrow 7\text{F}_2$  transition is of the hypersensitive type and strongly depends on the structure of the matter surrounding the europium ions [12,14–16].

Although the origins of transparent active GC doped with lanthanide ions date back to the 1970s [17] and optical fibers' the 1960s [11,18], GC still poses problems when drawing optical fibers. Glass-ceramics compromise quantum efficiency [19–21], which depends on the local environment around RE ions, the chemical composition, luminescence, and thermal properties. For applications where the target product will be fibers, the crystallization strategy should focus on nano-ceramic materials with maximum crystal sizes below 20 nm–30 nm to maintain good transmission properties of the material and avoid scattering on large crystals [2,4,22]. The material's thermal stability should also be kept in mind to obtain good quality fiber without unwanted crystallization connected with crystallization peaks [23,24]. The tested material meets many of the above postulates and has great potential for use as an optical fiber core. However, this may require further research and experimentation.

At present, there are several leading methods for the fabrication of active glass-ceramic materials. The first is direct doping involving the addition of crystals to the molten glass mass, and after quenching and annealing, manufactured material is a core material ready to be drawn in the rod-in-tube method. Unfortunately, the melting and, after that, the drawing process, degrades crystals [19,25]. Alternatively, the core material can be melted inside the cladding material, and this method is melt-in-tube (molten-core) or powder-in-tube [10,18,26,27]. This method of obtaining fibers involves diffusion problems between core and cladding materials, core irregularity and the difference between core and cladding in melting point, and viscosity [18]. The second classic method is based on manufacturing core bulk material. This material can have crystals or be grown in the heat treatment process [7,28,29]. Bulk material is the core material, but like in the first method, those crystals dissolve partially in the rod-in-tube drawing process. Alternatively, drawn optic fiber has an amorphous core, and crystals are grown in the heat treatment process after being drawn [10,18,26]. All these methods are characterized by the degradation of added crystals or problems with the amount and size of growth crystal, so more of these ways of obtaining optic fiber are multi-step and take a big amount of time on the heat treatment process [10,18,26]. An alternative to these methods should be the method based on obtaining the glass-ceramic structure in the process of fiber drawing.

Based on our earlier investigations, SGS glass was chosen for this investigation because of its good thermal stability, and low phonon energy glass matrix, which can improve quantum efficiency and probability of radiative transitions for electrons of rare-earth ion dopant [4,6,30]. Another reason was the possibility of shaping SGS into optic fibers. This research analyzed the effect of  $\text{P}_2\text{O}_5$  concentration on the luminescence spectra, asymmetry ratio (AR), and luminescence decay. Due to earlier work [30], we decided to limit the  $\text{P}_2\text{O}_5$  concentration up to 1 mol%, and we mainly focused on investigating the crystallization process in antimony-germanate-silicate glass, enabling size and density control of  $\text{EuPO}_4$  nanocrystals. The main objective of this experiment was to obtain a good optical quality core material as an 11 mm dia rod with specific crystalline properties and crystallization conditions.

## 2. Materials and Methods

Glasses with chemical composition (molar)  $35\text{SiO}_2 - 5\text{Al}_2\text{O}_3 - (29.5 - x)\text{GeO}_2 - 20\text{Sb}_2\text{O}_3 - 10\text{Na}_2\text{O} - x\text{P}_2\text{O}_5$ , (SGS) doped with  $0.5\text{Eu}_2\text{O}_3$ , where  $x = 0, 0.25, 0.5, 0.75$  and  $1$ , were prepared by the melting-quenching method. The set was prepared from Sigma-Aldrich materials of  $>99.99\%$  purity. The components were ground and homogenized in an agate mortar, and melted in an alumina crucible at  $1450\text{ }^\circ\text{C}$  by 2 h. Next, the molten material was poured into a brass mold to form 11 mm diameter rods. The bars were annealed at  $20\text{ }^\circ\text{C}$  below  $T_g$  for 8 h. In the next step, the rod was cut into 3 mm discs, which were polished to a final thickness of 2.5 mm. Some of the samples were subjected to the heat process, Samples were placed in a furnace preheated up to  $730\text{ }^\circ\text{C}$ . After the furnace temperature stabilized at  $730\text{ }^\circ\text{C}$  again, heating was turned off, and the furnace cooled down to room temperature in 7 h.

DSC measurement in the temperature range from  $200$  to  $1000\text{ }^\circ\text{C}$  was performed at  $10\text{ }^\circ\text{C}/\text{min}$  using the SETARAM Labsys thermal analyzer (Setaram Instrumentation, Caluire, France). X-ray diffraction studies were carried out on the X'Pert Pro X-ray diffractometer supplied by PANalytical (Eindhoven, The Netherlands) with  $\text{Cu K}\alpha_1$  radiation ( $\lambda = 1.54056\text{ \AA}$ ) in the  $2\theta$  range of  $5^\circ$ – $90^\circ$ . The step size, time per step, and scan speed were as follows:  $0.017^\circ$ ,  $184.79$ , and  $0.011^\circ/\text{s}$ . The X-ray tube was operated at  $40\text{ kV}$  and  $40\text{ mA}$ , and a scintillation detector was used to measure the intensity of the scattered X-rays.

The excitation and luminescence spectra of the glasses in a range of  $350$ – $750\text{ nm}$  were measured using the JobinYvon Fluoromax4 spectrophotometer (Horiba Jobin Yvon, Longjumeau, France). A system PTI QuantaMaster QM40 (Horiba Instruments, New York, NY, USA) coupled with a tunable pulsed optical parametric oscillator (OPO), pumped by the third harmonic of the Nd:YAG laser (OpotekOpolette 355 LD, Carlsbad, CA, USA), was used for luminescence decay measurements. The laser system was equipped with a double  $200\text{ mm}$  monochromator, a multimode UV-VIS PMT (R928), and Hamamatsu H10330B-75 detectors controlled by a computer. Luminescence decay curves were recorded and stored by a PTI ASOC-10 (USB-2500, Horiba Instruments, New York, NY, USA) oscilloscope with an accuracy of  $\pm 1\text{ }\mu\text{s}$ .

## 3. Results and Discussion

### 3.1. Differential Scanning Calorimetry

Figure 1 showed DSC curves where a small effect of phosphorous content on characteristic transformation temperature ( $T_g$ ) was observed. With the increasing  $\text{P}_2\text{O}_5$  content,  $T_g$  slightly decreases as well as crystallization temperature  $T_x$  increases. There are only weak exothermic changes, which indicate a low tendency to crystallization. Fabricated SGS glasses are characterized by good thermal stability, and this is also the case here, for there are weak exothermic changes that indicate a low tendency to crystallization [31].

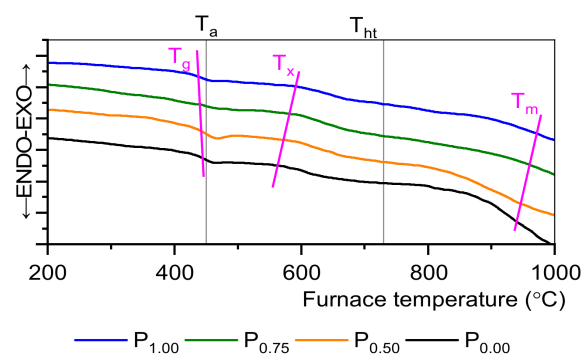


**Figure 1.** DSC curves. Temperatures:  $T_g$ —glass transition,  $T_{ht}$ —heat treatment,  $T_x$ —crystallization,  $T_a$ —annealing, and  $T_c$ —crystallization peak.

Analyzing reference glass without orthophosphate compound following formulas were used to calculate glass stability and crystals' nucleation and growth [23,32]:

$$\Delta T = T_x - T_g \quad (1)$$

$$H_r = \frac{T_x - T_g}{T_m - T_x} \quad (2)$$

$$T_{rg} = \frac{T_g}{T_m} \quad (3)$$

$$H' = \frac{T_x - T_g}{T_g} \quad (4)$$

where  $\Delta T$  reflects the glass's devitrification tendency and has a factor from 117 °C for the sample without orthophosphate to 155 °C for a 1 mol%  $P_2O_5$  sample. A thermal stability factor  $\Delta T$  higher than 100 °C is a good indication for the possibility of drawing fibers from such a material [6,16,33]. Hruby's parameter  $H_r$  is 0.28 for the reference sample and 0.44 for 1 mol% of the  $P_2O_5$  sample and gives information on the nucleation rate of the crystals [34]. The range of  $T_x - T_g$  is connected with a viscosity of melted material, and a wider gap means lower viscosity. Additionally, range  $T_m - T_x$  is connected with crystal growth rate, for narrow gap crystal growth rate slows rapidly [34]. Simplified Hruby's parameter  $H'$  is 0.26 for the reference sample and 0.35 for a 1 mol%  $P_2O_5$  sample, which confirms good thermal stability [16,23]. When  $T_{rg}$  is lower than 0.75 is a good mark of the homogenous crystal nucleation in volume, where  $T_{rg} > 0.75$  could indicate surface crystallization [32]. In this case, for the undoped sample  $T_{rg} = 0.45$  and for 1 mol%, the  $P_2O_5$  is 0.59. In general, the DSC study demonstrated a slight decrease in  $T_g$  point with increasing nucleator concentration due to a lower phosphorous melting temperature. On the other hand,  $T_x$  increases, which can be related to the increasing tendency to crystallize the material.

### 3.2. X-ray Diffraction

X-ray diffraction research was performed to determine the structural changes of prepared glass and glass-ceramic. Table 1, based on patterns (Supplementary Materials Figures S1–S5), summarizes the Sherrer formula estimates of the crystals obtained at several observed  $2\theta$  angles for the glasses before and after heat treatment. Based on the data analysis, it was observed that for samples doped with 0.25 mol%  $P_2O_5$ , the first nanometric crystallites appeared after heat treatment. An increase of  $P_2O_5$  content to 0.5 mol% deepens the degree of crystallization, resulting in new reflections at  $2\theta = 42^\circ$  and  $72^\circ$ . In both samples, no crystallization was observed before heat treatment. Some surprise is the presence of large  $> 65$  nm crystallites in the sample with 0.5 mol% phosphorous. Further increasing the  $P_2O_5$  content up to 0.75 mol% results in the formation of crystallites in samples before heat treatment. A slight increase in crystallite size was observed around  $2\theta = 30^\circ$  and more significant growth at  $2\theta = 32^\circ$ . Material with 1 mol% nucleator doping resulted in large crystallites above 20 nm and the appearance of new nanocrystallites for  $26^\circ$ .

For all cases where crystals were present, they were identified as monoclinic  $EuPO_4$  crystals (reference code 00-025-1055). In the  $EuPO_4$  crystal lattice, europium ions are coordinated with Eu-O and P-O atoms bonds forming polyhedrons [35,36]. In our experiment, the bulk crystallization mechanism was observed [37,38].

### 3.3. Excitation Spectra

Excitation spectra studies at two wavelengths, 590 nm and 612 nm, were performed to determine the effect of the molar content of nucleator ions and the heat treatment process on the excitation bands as a function of  $P_2O_5$  concentration. The excitation spectra of the fabricated samples were measured for emission monitored at the wavelengths of 590 nm (Figure 2) and 612 nm (Figure 3), corresponding to magnetic dipole and electric-dipole

transitions, respectively. In both cases, seven bands were observed on the examination spectrum at wavelengths: 360, 380, 395, 415, 465, 528, and 535 nm. Specific excitation bands may be combined with a magnetic (MD) or electric dipole (ED). Moreover, they can be connected to hypersensitive transitions. In this case, the most interesting transitions are described as hypersensitive and environment independent. Table 2 presents the chosen transition to analyzing examined samples [14].

**Table 1.** XRD table crystallite size depends on theta angle, nucleator concentration, and heat treatment process (all crystallite sizes in nm).

| P <sub>2</sub> O <sub>5</sub> Nucleator Concentration | 0.25 mol% |                  | 0.50 mol%        |     | 0.75 mol% |       | 1.0 mol% |       |       |
|---|-----------|------------------|------------------|-----|-----------|-------|----------|-------|-------|
|   | 2θ        | Bht <sup>1</sup> | Aht <sup>2</sup> | Bht | Aht       | Bht   | Aht      | Bht   | Aht   |
| 26  |           |                  |                  |     |           |       |          |       | 5.82  |
| 28  |           |                  |                  |     |           |       | 20.66    |       | 8.26  |
| 30  |           |                  | 12.53            |     | 16.27     | 14.28 | 15.89    | 22.75 | 30.95 |
| 32  |           |                  | 11.49            |     | 15.85     | 16.92 | 27.24    |       | 43.93 |
| 42  |           |                  |                  |     | 65.50     |       |          |       |       |
| 72  |           |                  |                  |     | 28.18     |       |          |       |       |

<sup>1</sup> Bht—Before heat treatment; <sup>2</sup> Aht—After heat treatment.

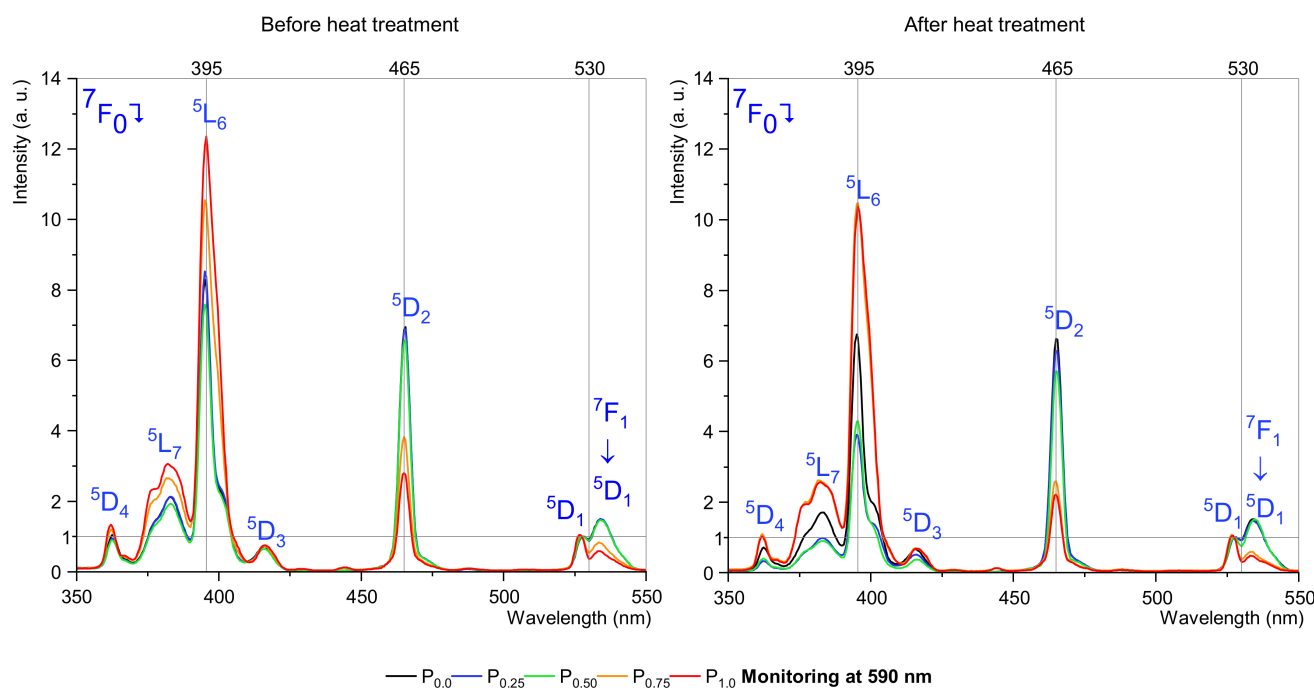


**Figure 2.** Excitation spectra, monitoring at 590 nm.

**Table 2.** The chosen transitions of Eu<sup>3+</sup> ions.

| Transition                    | Dipole Type | Wavelength Range (nm) | Transition Describes                     |
|-------------------------------|-------------|-----------------------|--|
| ${}^7F_0 \rightarrow {}^5L_6$ | ED          | 390–405               | Most intense transition                  |
| ${}^7F_0 \rightarrow {}^5D_2$ | ED          | 460–470               | Hypersensitive transition                |
| ${}^7F_0 \rightarrow {}^5D_1$ | MD          | 520–530               | Intensity independent of the environment |
| ${}^7F_1 \rightarrow {}^5D_1$ | ED          | 530–540               | Hypersensitive transition                |

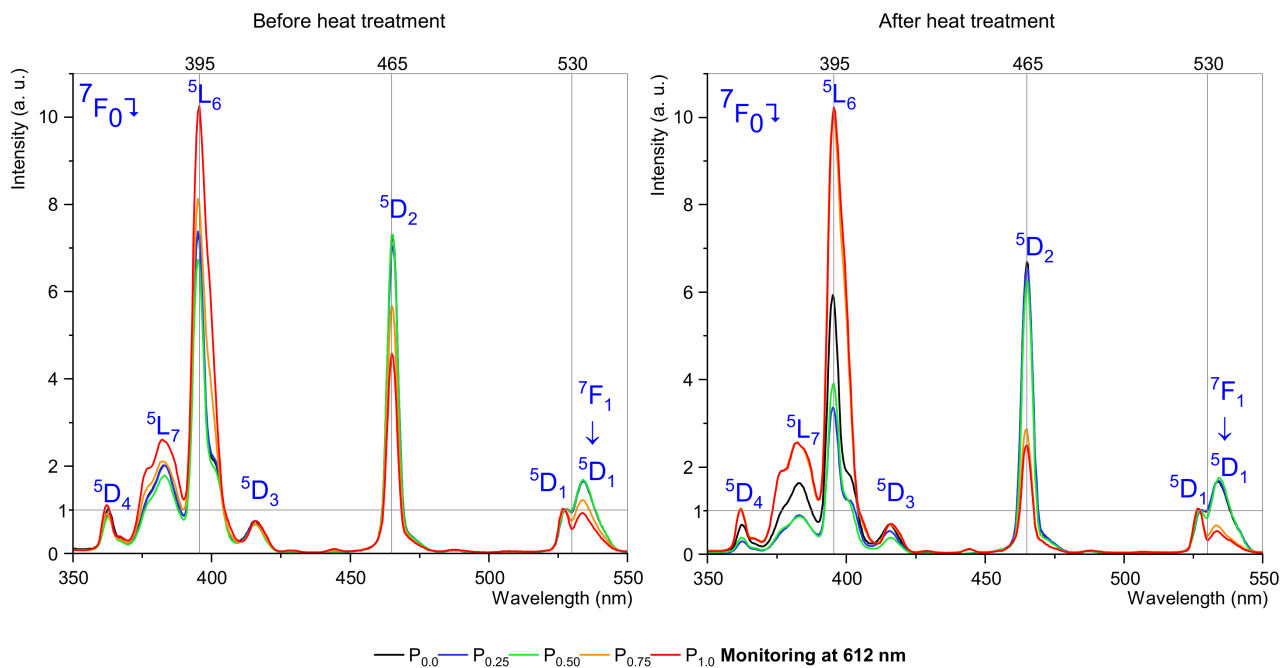


**Figure 3.** Excitation spectra, monitoring at 612 nm.

Figures 2 and 3 show excitation spectra normalized by  ${}^7F_0 \rightarrow {}^5D_1$  transition, which is environment independent, making it possible to observe changes in the most interfering excitation bands, i.e., 395 nm and 465 nm.

According to excitation spectra analysis monitoring at 590 nm, we observed that the highest intensity band and the hypersensitive bands show some rules, with hypersensitive transitions ( ${}^7F_0 \rightarrow {}^5D_2$  and  ${}^7F_1 \rightarrow {}^5D_1$ ) decreasing their intensity with orthophosphate concentration, and this effect has a slight change between the heat treatment sample and before the heat treatment sample. Therefore, with more, up to 0.5 mol%  $P_2O_5$  concentration, there are almost no changes in intensity compared to the reference sample (without  $P_2O_5$ ), but with 0.75 mol% of the  $P_2O_5$  threshold intensity declining rapidly. A different situation is with the  ${}^7F_0 \rightarrow {}^5L_6$  transition, their intensity increases with the concentration raise of orthophosphate. The 395 nm band changes after heat treatment, low doped by  $P_2O_5$  samples strongly decreasing in intensity, contrary to the 0.75 mol% and 1.0 mol% doped samples decreasing slightly.

In the case of excitation spectra monitored at 612 nm, the analysis shows similar behavior to spectra monitored at 590 nm but with some differences in intensity linked with the heat treatment process. Therefore, more interesting maximum intensities of 390–405 nm and 460–470 nm bands were almost unchanged after heat treatment. This effect and changes for the 395 and 465 nm band confirm that the europium ions are in the crystalline phase. Surprisingly, there was a strong change in the intensity for the  ${}^7F_0 \rightarrow {}^5D_1$  transition in the annealed samples. This transition, similarly to the hypersensitive  ${}^7F_0 \rightarrow {}^5D_2$  transition, is strongly dependent on environment structure. The study confirmed the change in the structure of the samples, both as a function of annealing and nucleator content.

### 3.4. Luminescence Investigation and Decay

According to the results, we decided to use both excitation bands for further study on luminescence and decay. The main objective of the luminescence studies was to confirm that the luminescence changes depend on the  $P_2O_5$  concentration, which is a confirmation of the incorporation of europium ions into the crystal structure. Similar to excitation spectra, there are also hypersensitive and independent of environment transitions. Selected information about that phenomena are in Table 3 [12,14,39–41].

**Table 3.** The selected radiative transitions of  $\text{Eu}^{3+}$  ions.

| Transition                                  | Dipole Type | Wavelength Range (nm) | Transition Describes                             |
|---|-------------|-----------------------|--|
| ${}^5\text{D}_0 \rightarrow {}^7\text{F}_1$ | MD          | 585–600               | Intensity largely independent of the environment |
| ${}^5\text{D}_0 \rightarrow {}^7\text{F}_2$ | ED          | 610–630               | Hypersensitive                                   |
| ${}^5\text{D}_0 \rightarrow {}^7\text{F}_4$ | ED          | 680–710               | Sensitive, depend on environment                 |

The  ${}^5\text{D}_0 \rightarrow {}^7\text{F}_1$  transition is observed to be magnetic dipole dependent while, at the same time, the transition is independent of the structure of the matter surrounding the europium ions. Therefore, the luminescence in this band was normalized and used as a reference. In contrast, the  ${}^5\text{D}_0 \rightarrow {}^7\text{F}_2$  transition depends on the structure of matter around the europium ions. By comparing the luminescence for the  ${}^5\text{D}_0 \rightarrow {}^7\text{F}_1$  and  ${}^5\text{D}_0 \rightarrow {}^7\text{F}_2$  transitions, the asymmetry factor can be determined, which allows us to assume the presence of lanthanide ions in the crystal lattice. For this purpose, the incident results were processed using the formula [12,16,42]:

$$\text{asymmetry ratio} = \frac{\int_{604\text{nm}}^{632\text{nm}} {}^5\text{D}_0 \rightarrow {}^7\text{F}_2}{\int_{582\text{nm}}^{604\text{nm}} {}^5\text{D}_0 \rightarrow {}^7\text{F}_1} \quad (5)$$

The study was conducted for two selected excitation wavelengths: 395 nm (Figure 4) and 465 nm (Figure 5) before and after the heat treatment process.

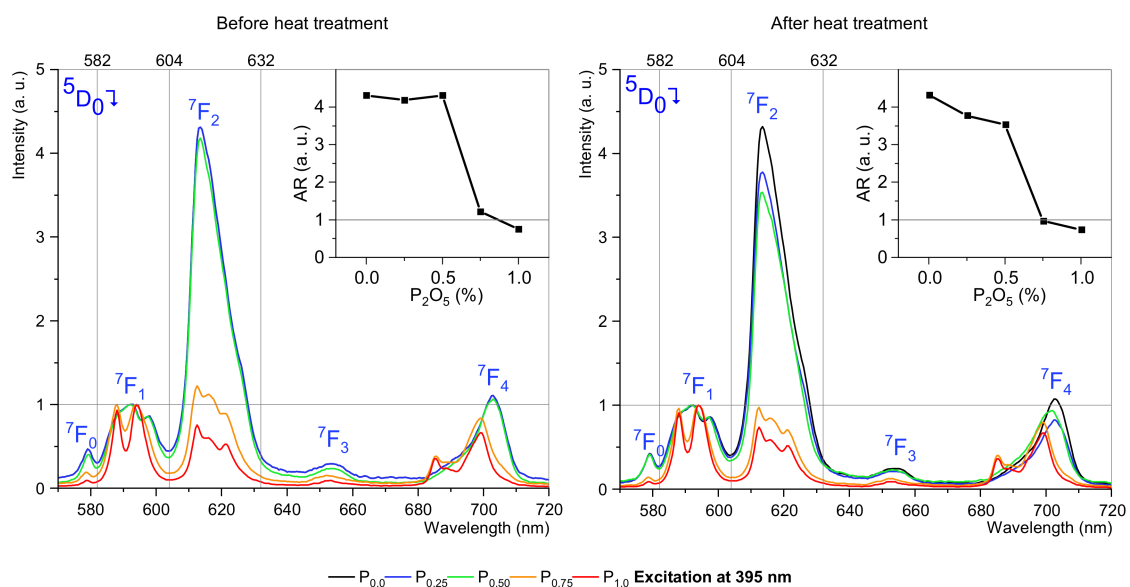


**Figure 4.** Luminescence spectra of SGS glasses doped with 0.5 mol%. In insets, asymmetry ratios are as a function of  $\text{P}_2\text{O}_5$  concentration.

In the first analyzed case, it was observed that for excitation at 395 nm, the  ${}^5\text{D}_0 \rightarrow {}^7\text{F}_2$  transition strongly depends on the concentration of  $\text{P}_2\text{O}_5$ . The phosphorus oxide content up to 0.5 mol% hardly changes the luminescence compared to the sample without phosphorus oxide, but higher concentrations strongly change the luminescence spectrum, especially the  ${}^5\text{D}_0 \rightarrow {}^7\text{F}_2$  transition. Due to the 612 nm band being hypersensitive and strongly depending on the environment, such a change is a strong signal, indicating structural changes around  $\text{Eu}^{3+}$  ions. After the heat-treatment process, the luminescence changes are even more profound. There are interesting changes for the  ${}^5\text{D}_0 \rightarrow {}^7\text{F}_1$  transition, where a change of active sublevels (Stark's effect) can be observed and resulting from changes in the structure of matter surrounding the europium ions. Usually,  ${}^5\text{D}_0 \rightarrow {}^7\text{F}_1$  splits into three Stark's sublevels when the ion is located in a low symmetry site [12], and this situation is

observed for concentrations up to 0.5 mol%  $P_2O_5$ . For higher concentrations of phosphorus oxide,  $^5D_0 \rightarrow ^7F_1$  splits into two sublevels. Changes in luminescence in the test samples are translated into changes in the asymmetry ratio. Between phosphorus oxide concentrations are 0.5 mol% and 0.75 mol% the asymmetry ratio (AR) decline rapidly.

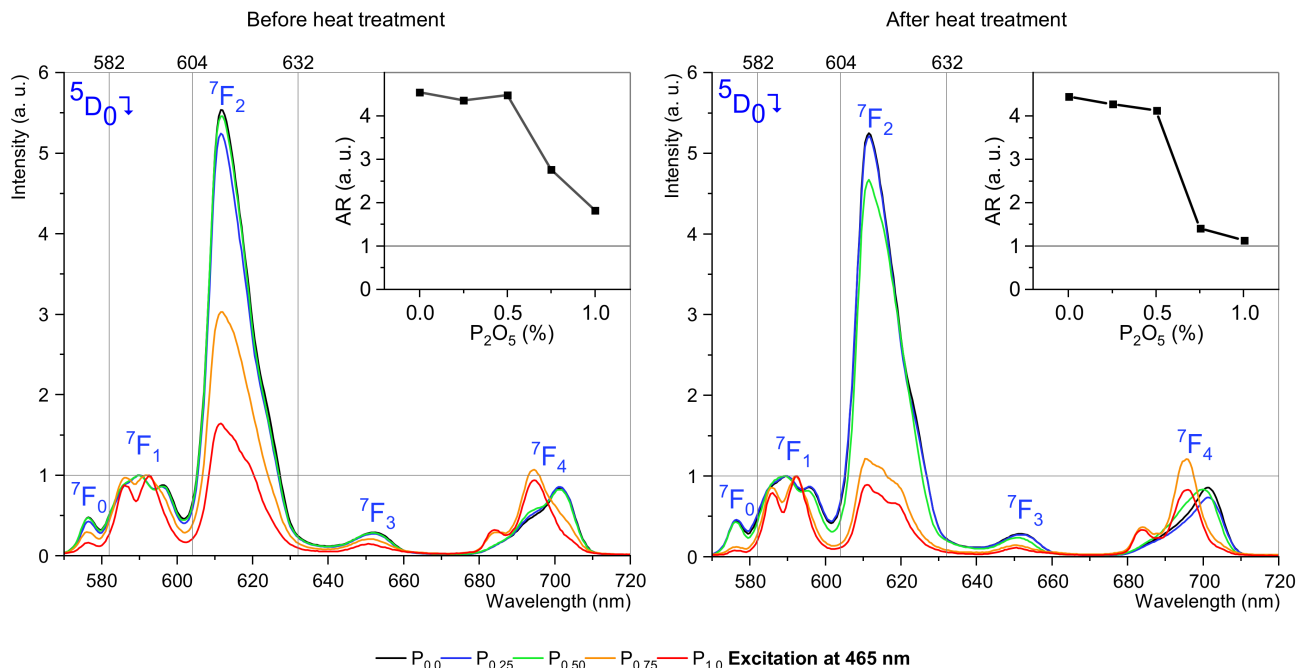


**Figure 5.** Luminescence spectra of SGS glasses doped with 0.5 mol%  $Eu_2O_3$ . In insets, asymmetry ratios as a function of  $P_2O_5$  concentration.

The luminescence under 464 nm has the highest intensity and the most dominant ED transition (Figure 5). The different emission profiles propose that the site-selective luminescence is possible in fabricated glass-ceramic. The emission spectra confirm the occupancy of  $Eu^{3+}$  ions at different crystallographic environments with varying asymmetric ratios. To better understand the mechanisms of crystallization of  $EuPO_4$  nanocrystals, the luminescence decay at two excitation channels are analyzed in detail. Figures 6 and 7 show that glasses without or 0.25 mol%  $P_2O_5$  content are purely amorphous. However, fabricated glasses where  $P_2O_5$  content is higher than 0.5 mol% show a composite structure, which indicates the presence of crystals. This is particularly evident in samples with 0.75 mol% and 1.0 mol% phosphorus content. For amorphous materials, the results are approximated by a single-exponential function, while the appearance of crystalline structures requires a dual-exponential function [4,43]. Data from the experiment were fitted by the following equation:

$$I(t) = A_1 \exp\left(-\frac{t}{\tau_1}\right) + A_2 \exp\left(-\frac{t}{\tau_2}\right) \quad (6)$$

To more easily compare lifetimes of different samples, the averaged observed lifetimes were calculated with the formula:

$$\tau_{avg} = \frac{A_1 \tau_1^2 + A_2 \tau_2^2}{A_1 \tau_1 + A_2 \tau_2} \quad (7)$$

where  $\tau_1$  and  $\tau_2$  are long and short luminescence lifetime components, and  $A_1$  and  $A_2$  are constants amplitudes of respective decay components. The double-exponential character of the decay curves indicates the presence of two different surroundings of europium ions. Long lifetime  $\tau_1$  corresponds to higher symmetry of the crystal field, while short lifetime  $\tau_2$  is connected with lower symmetry of the  $Eu^{3+}$  surroundings [4,12,43].

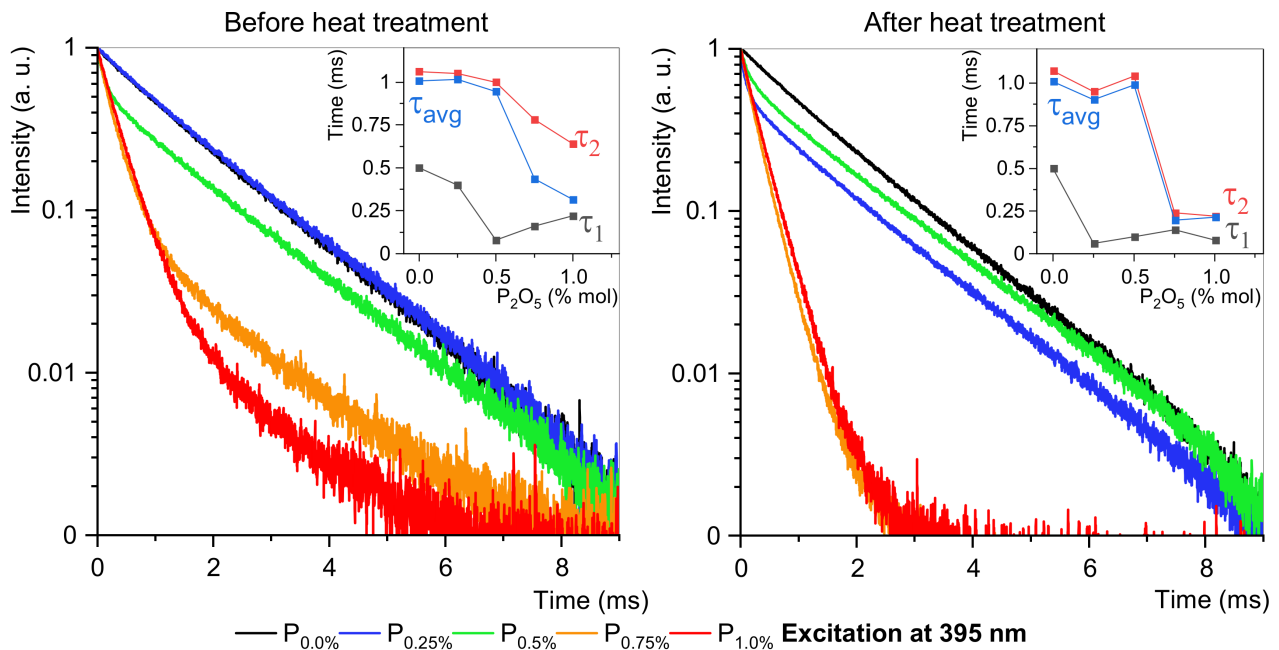


**Figure 6.** Luminescence decays and  $\tau$  changes at 395 nm excitation. Lifetimes are in insets.

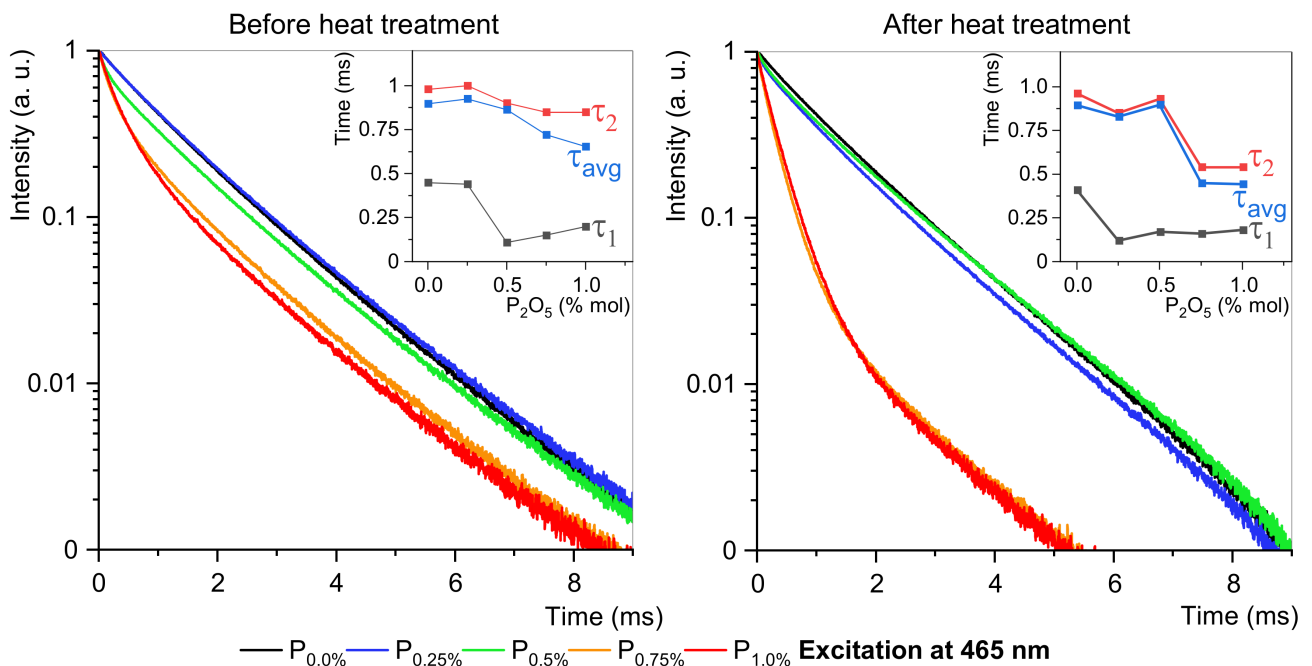


**Figure 7.** Luminescence decays and  $\tau$  changes at 465 nm excitation. Lifetimes are in insets.

As in previous studies, this study also confirmed a change in the structure of the matter surrounding the  $\text{Eu}^{3+}$  ions. Tables 4 and 5 show that two concentrations are critical 0.5 mol% and 0.75 mol%  $\text{P}_2\text{O}_5$ . Excitation at 395 nm shows that sample  $P_{0.5}$  is the first double exponential, and  $\tau_1$  changes rapidly because of a new relaxation channel. For 0.5 mol%  $\text{P}_2\text{O}_5$  concentrations and higher,  $\tau_1$  grows slowly, and  $\tau_2$  decreases. After heat treatment,  $\tau_2$  changes fast, and it is almost flattered for  $P_{0.75}$  and  $P_{1.0}$  samples.

**Table 4.** Lifetime of  $^5D_0$  level at excitation of 395 nm.

| Sample            | Before Heat Treatment, Excited at 395 nm |               |                |               |                   |                | After Heat Treatment, Excited at 395 nm |               |                |               |                   |                |
|-------------------|--|---------------|----------------|---------------|-------------------|----------------|---|---------------|----------------|---------------|-------------------|----------------|
|                   | A <sub>1</sub>                           | $\tau_1$ [ms] | A <sub>2</sub> | $\tau_2$ [ms] | $\tau_{avg}$ [ms] | R <sup>2</sup> | A <sub>1</sub>                          | $\tau_1$ [ms] | A <sub>2</sub> | $\tau_2$ [ms] | $\tau_{avg}$ [ms] | R <sup>2</sup> |
| P <sub>0.0</sub>  | 0.97                                     | 0.97          |                |               | 0.97              | 0.9998         | 0.99                                    | 0.94          |                |               | 0.94              | 0.9996         |
| P <sub>0.25</sub> | 0.98                                     | 0.96          |                |               | 0.96              | 0.9997         | 0.63                                    | 0.72          |                |               | 0.72              | 0.9703         |
| P <sub>0.5</sub>  | 0.44                                     | 0.08          | 0.54           | 1.00          | 0.9437            | 0.9995         | 0.37                                    | 0.10          | 0.63           | 1.04          | 0.9897            | 0.9997         |
| P <sub>0.75</sub> | 0.85                                     | 0.16          | 0.14           | 0.78          | 0.7361            | 0.9996         | 0.58                                    | 0.14          | 0.43           | 0.24          | 0.1959            | 0.9999         |
| P <sub>1.0</sub>  | 0.89                                     | 0.22          | 0.09           | 0.64          | 0.3154            | 0.9998         | 0.11                                    | 0.08          | 0.9            | 0.22          | 0.2140            | 0.9998         |

**Table 5.** Lifetime of  $^5D_0$  level at excitation of 465 nm.

| Sample            | Before Heat Treatment, Excited at 465 nm |               |                |               |                   |                | After Heat Treatment, Excited at 465 nm |               |                |               |                   |                |
|-------------------|--|---------------|----------------|---------------|-------------------|----------------|---|---------------|----------------|---------------|-------------------|----------------|
|                   | A <sub>1</sub>                           | $\tau_1$ [ms] | A <sub>2</sub> | $\tau_2$ [ms] | $\tau_{avg}$ [ms] | R <sup>2</sup> | A <sub>1</sub>                          | $\tau_1$ [ms] | A <sub>2</sub> | $\tau_2$ [ms] | $\tau_{avg}$ [ms] | R <sup>2</sup> |
| P <sub>0.0</sub>  | 0.98                                     | 0.83          |                |               | 0.83              | 0.9993         | 0.98                                    | 0.82          |                |               | 0.82              | 0.9994         |
| P <sub>0.25</sub> | 0.97                                     | 0.86          |                |               | 0.86              | 0.9993         | 0.89                                    | 0.76          |                |               | 0.76              | 0.9975         |
| P <sub>0.5</sub>  | 0.28                                     | 0.11          | 0.71           | 0.90          | 0.8636            | 0.9998         | 0.91                                    | 0.81          |                |               | 0.81              | 0.9974         |
| P <sub>0.75</sub> | 0.55                                     | 0.15          | 0.43           | 0.85          | 0.7210            | 0.9998         | 0.82                                    | 0.16          | 0.77           | 0.54          | 0.4488            | 0.9998         |
| P <sub>1.0</sub>  | 0.64                                     | 0.20          | 0.35           | 0.85          | 0.6455            | 0.9998         | 0.86                                    | 0.18          | 0.78           | 0.54          | 0.4432            | 0.9999         |

Excitation at 465 nm before heat treatment is analogous to excitation at 395 nm before heat treatment. A different situation is that after heat treatment, a known edge at 395 nm for 0.5 mol% P<sub>2</sub>O<sub>5</sub> concentration moves to 0.75 mol% P<sub>2</sub>O<sub>5</sub> concentration. Flattered zones for 0.75 mol% and 1.0 mol% concentrations of P<sub>2</sub>O<sub>5</sub> are informative about the maximum concentration of P<sub>2</sub>O<sub>5</sub>. Therefore, higher concentrations of orthophosphoric will not significantly affect the shortened lifetime.

#### 4. Conclusions

In this study, we determined the mechanism of crystallization of EuPO<sub>4</sub> nanocrystals located in antimony-germanate-silicate glass. Luminescence and excitation studies indicate that samples with 0.5 mol% P<sub>2</sub>O<sub>5</sub> and higher concentration are characterized by a lower asymmetry ratio in the excitation scheme at 394 nm. It was noticed that the local symmetry exists in the vicinity of Eu<sup>3+</sup> ions in this sample. Based on XRD measurements, nanocrystals with sizes in the range of 20–40 nm were found in almost all the glass samples tested. Moreover, the lifetime studies confirm the critical concentration of P<sub>2</sub>O<sub>5</sub>, where we can clearly see a sharp decrease in lifetimes for concentrations of 0.5–0.75 mol% P<sub>2</sub>O<sub>5</sub>. It is also easy to see that the dynamics of change is much higher for 394 nm excitation and for annealed samples. The rapid change in  $\tau_2$  also indicates energy dissipation on large crystals, which behave as optical dimmers.

By proceeding with the investigation, the results were assumed that the material after melting should be amorphous, without crystals, while after heat treatment, the structure should change from amorphous to GC. The fabricated material meets many of the above postulates and has great potential for use as an optical fiber core, which is confirmed by thermal stability (DSC), X-ray analysis (XRD), and spectroscopic measurements. In the course of this study, it appears that SGS samples from a 0.25 mol% to 0.75 mol% nucleator concentration seem to be the most interesting in terms of the changes occurring in them and in terms of the strategy of obtaining nano-ceramic. However, in terms of the possibility of obtaining glass-ceramics in the form of optical fibers, the range of 0.25 mol% to 0.5 mol% P<sub>2</sub>O<sub>5</sub> seems to be a better choice in terms of the dynamics of changes and thus the stability of the one-step process under development. As mentioned in the introduction, glass-ceramics are still under challenge, hence the fabricated antimony-germanate-silicate glass-ceramic is a compromise between luminescent properties and fiber drawing ability.

**Supplementary Materials:** The following supporting information can be downloaded at: <https://www.mdpi.com/article/10.3390/ma15113797/s1>. Figure S1: XRD patterns of SGS (without P<sub>2</sub>O<sub>5</sub>); Figure S2: XRD patterns of SGS (with 0.25% P<sub>2</sub>O<sub>5</sub>); Figure S3: XRD patterns of SGS (with 0.5% P<sub>2</sub>O<sub>5</sub> dope); Figure S4: XRD patterns of SGS (with 0.75% P<sub>2</sub>O<sub>5</sub> dope); Figure S5: XRD patterns of SGS (with 1.0% P<sub>2</sub>O<sub>5</sub> dope).

**Author Contributions:** Conceptualization, J.Ż., D.D.; methodology, M.L., M.K. (Marta Kuwik), T.R., K.S. and P.M.; formal analysis, M.K. (Marcin Kochanowicz), P.M., J.Ż. and W.P.; investigation and data curation, P.G., T.R. and K.S.; writing—review and editing, J.D., J.Ż., W.P. and J.P.; visualization, P.G., M.L. and M.K. (Marta Kuwik); supervision, J.Ż. and M.K. (Marcin Kochanowicz), D.D., J.P. and J.D.; project administration, J.Ż. All authors have read and agreed to the published version of the manuscript.

**Funding:** This research was funded by the National Science Centre (Poland) granted on the basis of decision No. DEC-2019/35/O/ST5/03105. The APC was funded by Białystok University of Technology.

**Institutional Review Board Statement:** Not applicable.

**Informed Consent Statement:** Not applicable.

**Data Availability Statement:** Not applicable.

**Conflicts of Interest:** The authors declare no conflict of interest.

## References

1. Zhao, L.; Cao, Z.; Wei, X.; Yin, M.; Chen, Y. Luminescence Properties of Eu<sup>3+</sup> Doped YBO<sub>3</sub> for Temperature Sensing. *J. Rare Earths* **2017**, *35*, 356–360. [[CrossRef](#)]
2. Kang, S.; Dong, G.; Qiu, J.; Yang, Z. Hybrid Glass Optical Fibers—Novel Fiber Materials for Optoelectronic Application. *Opt. Mater. X* **2020**, *6*, 100051. [[CrossRef](#)]
3. Klimesz, B.; Lisiecki, R.; Ryba-Romanowski, W. Thermosensitive Tm<sup>3+</sup>/Yb<sup>3+</sup> Co-Doped Oxyfluorotellurite Glasses—Spectroscopic and Temperature Sensor Properties. *J. Alloy. Compd.* **2020**, *823*, 153753. [[CrossRef](#)]
4. Milewska, K.; Maciejewski, M.; Synak, A.; Łapiński, M.; Mielewczyk-Gryń, A.; Sadowski, W.; Kościelska, B. From Structure to Luminescent Properties of B<sub>2</sub>O<sub>3</sub>-Bi<sub>2</sub>O<sub>3</sub>-SrF<sub>2</sub> Glass and Glass-Ceramics Doped with Eu<sup>3+</sup> Ions. *Materials* **2021**, *14*, 4490. [[CrossRef](#)] [[PubMed](#)]
5. Ren, J.; Ren, J.; Lu, X.; Lin, C.; Lin, C.; Jain, R.K.; Jain, R.K. Luminescent Ion-Doped Transparent Glass Ceramics for Mid-Infrared Light Sources [Invited]. *Opt. Express OE* **2020**, *28*, 21522–21548. [[CrossRef](#)]
6. Yatskiv, R.; Kostka, P.; Grym, J.; Zavadil, J. Temperature Sensing down to 4 K with Erbium-Doped Tellurite Glasses. *J. Non-Cryst. Solids* **2022**, *575*, 121183. [[CrossRef](#)]
7. Yu, B.; Zheng, B.; Xia, H.; Wang, J.; Song, H.; Chen, B. Tunable Emission and Temperature Sensing Performance in Novel Oxyfluoride Borosilicate Glass Ceramics Containing Eu<sup>3+</sup>/Tb<sup>3+</sup>: KY3F10 Nanocrystals. *Ceram. Int.* **2021**, *47*, 9668–9678. [[CrossRef](#)]
8. Baranowska, A.; Leśniak, M.; Kochanowicz, M.; Żmojda, J.; Miluski, P.; Dorosz, D. Crystallization Kinetics and Structural Properties of the 45S5 Bioactive Glass and Glass-Ceramic Fiber Doped with Eu<sup>3+</sup>. *Materials* **2020**, *13*, 1281. [[CrossRef](#)]
9. Rudenko, M.; Gaponenko, N.; Litvinov, V.; Ermachikhin, A.; Chubenko, E.; Borisenko, V.; Mukhin, N.; Radyush, Y.; Tumarkin, A.; Gagarin, A. Structural Dependent Eu<sup>3+</sup> Luminescence, Photoelectric and Hysteresis Effects in Porous Strontium Titanate. *Materials* **2020**, *13*, 5767. [[CrossRef](#)]
10. Tian, X.; Ma, Z.; Qiu, J.; Wei, R. Nd<sup>3+</sup>-Doped Glass-Ceramic Fiber Fabricated by Drawing Precursor Ceramic and Successive Heat Treatment. *Ceram. Int.* **2022**; *in press*. [[CrossRef](#)]
11. Veber, A.; Lu, Z.; Vermillac, M.; Pigeonneau, F.; Blanc, W.; Petit, L. Nano-Structured Optical Fibers Made of Glass-Ceramics, and Phase Separated and Metallic Particle-Containing Glasses. *Fibers* **2019**, *7*, 105. [[CrossRef](#)]
12. Tran, T.N.L.; Chiasera, A.; Lukowiak, A.; Ferrari, M. Eu<sup>3+</sup> as a Powerful Structural and Spectroscopic Tool for Glass Photonics. *Materials* **2022**, *15*, 1847. [[CrossRef](#)]
13. Ćirić, A.; Stojadinović, S.; Brik, M.G.; Dramićanin, M.D. Judd-Ofelt Parametrization from Emission Spectra: The Case Study of the Eu<sup>3+</sup> 5D1 Emitting Level. *Chem. Phys.* **2020**, *528*, 110513. [[CrossRef](#)]
14. Binnemans, K. Interpretation of Europium(III) Spectra. *Coord. Chem. Rev.* **2015**, *295*, 1–45. [[CrossRef](#)]
15. Hui, Y.; Zhao, Y.; Zhao, S.; Gu, L.; Fan, X.; Zhu, L.; Zou, B.; Wang, Y.; Cao, X. Fluorescence of Eu<sup>3+</sup> as a Probe of Phase Transformation of Zirconia. *J. Alloys Compd.* **2013**, *573*, 177–181. [[CrossRef](#)]
16. Otsuka, T.; Brehl, M.; Cicconi, M.R.; de Ligny, D.; Hayakawa, T. Thermal Evolutions to Glass-Ceramics Bearing Calcium Tungstate Crystals in Borate Glasses Doped with Photoluminescent Eu<sup>3+</sup> Ions. *Materials* **2021**, *14*, 952. [[CrossRef](#)]

17. Auzel, F.; Pecile, D.; Morin, D. Rare Earth Doped Vitroceramics: New, Efficient, Blue and Green Emitting Materials for Infrared Up-Conversion. *J. Electrochem. Soc.* **1975**, *122*, 101–107. [[CrossRef](#)]
18. Yang, S.; Heyl, H.; Homa, D.; Pickrell, G.; Wang, A. Powder-in-Tube Reactive Molten-Core Fabrication of Glass-Clad BaO-TiO<sub>2</sub>-SiO<sub>2</sub> Glass-Ceramic Fibers. *Materials* **2020**, *13*, 395. [[CrossRef](#)]
19. Nguyen, H.; Tuomisto, M.; Oksa, J.; Salminen, T.; Lastusaari, M.; Petit, L. Upconversion in Low Rare-Earth Concentrated Phosphate Glasses Using Direct NaYF<sub>4</sub>:Er<sup>3+</sup>, Yb<sup>3+</sup> Nanoparticles Doping. *Scr. Mater.* **2017**, *139*, 130–133. [[CrossRef](#)]
20. Skaudzius, R.; Katelnikovas, A.; Enseling, D.; Kareiva, A.; Jüstel, T. Dependence of the 5D<sub>0</sub>→7F<sub>4</sub> Transitions of Eu<sup>3+</sup> on the Local Environment in Phosphates and Garnets. *J. Lumin.* **2014**, *147*, 290–294. [[CrossRef](#)]
21. Grigorjevaite, J.; Ezerskyte, E.; Minderyte, A.; Stanionyte, S.; Juskenas, R.; Sakirzanovas, S.; Katelnikovas, A. Optical Properties of Red-Emitting Rb<sub>2</sub>Bi(PO<sub>4</sub>)(MoO<sub>4</sub>):Eu<sup>3+</sup> Powders and Ceramics with High Quantum Efficiency for White LEDs. *Materials* **2019**, *12*, 3275. [[CrossRef](#)] [[PubMed](#)]
22. Ma, X.; Li, X.; Li, J.; Genevois, C.; Ma, B.; Etienne, A.; Wan, C.; Véron, E.; Peng, Z.; Allix, M. Pressureless Glass Crystallization of Transparent Yttrium Aluminum Garnet-Based Nanoceramics. *Nat. Commun.* **2018**, *9*, 1175. [[CrossRef](#)] [[PubMed](#)]
23. Pisarska, J.; Kaczmarczyk, B.; Mazurak, Z.; Zelechower, M.; Goryczka, T.; Pisarski, W.A. Influence of P<sub>2</sub>O<sub>5</sub> Concentration on Structural, Thermal and Optical Behavior of Pr-Activated Fluoroindate Glass. *Phys. B Condens. Matter* **2007**, *388*, 331–336. [[CrossRef](#)]
24. Santos Barbosa, J.; Batista, G.; Danto, S.; Fargin, E.; Cardinal, T.; Poirier, G.; Castro Cassanjes, F. Transparent Glasses and Glass-Ceramics in the Ternary System TeO<sub>2</sub>-Nb<sub>2</sub>O<sub>5</sub>-PbF<sub>2</sub>. *Materials* **2021**, *14*, 317. [[CrossRef](#)]
25. Ojha, N.; Tuomisto, M.; Lastusaari, M.; Petit, L. Phosphate Glasses with Blue Persistent Luminescence Prepared Using the Direct Doping Method. *Opt. Mater.* **2019**, *87*, 151–156. [[CrossRef](#)]
26. Fang, Z.; Zheng, S.; Peng, W.; Zhang, H.; Ma, Z.; Dong, G.; Zhou, S.; Chen, D.; Qiu, J. Ni<sup>2+</sup> Doped Glass Ceramic Fiber Fabricated by Melt-in-Tube Method and Successive Heat Treatment. *Opt. Express OE* **2015**, *23*, 28258–28263. [[CrossRef](#)]
27. Ballato, J.; Peacock, A.C. Molten Core Optical Fiber Fabrication—A Route to New Materials and Applications. *APL Photonics* **2018**, *3*, 120903. [[CrossRef](#)]
28. Wang, L.; Liu, J.; Lu, N.; Yang, Z.; He, G.; Li, X.; Li, J.; Li, J. Synthesis and Crystallization Kinetics of Y<sub>2</sub>CaAl<sub>4</sub>SiO<sub>12</sub> Garnet-Type Glass-Ceramic. *Scr. Mater.* **2020**, *188*, 222–227. [[CrossRef](#)]
29. Ojha, N.; Szczodra, A.; Boetti, N.G.; Massera, J.; Petit, L. Nucleation and Growth Behavior of Er<sup>3+</sup> doped Oxyfluorophosphate Glasses. *RSC Adv.* **2020**, *10*, 25703–25716. [[CrossRef](#)]
30. Zmojda, J.; Kochanowicz, M.; Miluski, P.; Baranowska, A.; Pisarski, W.A.; Pisarska, J.; Jadach, R.; Sitarz, M.; Dorosz, D. Optical Characterization of Nano- and Microcrystals of EuPO<sub>4</sub> Created by One-Step Synthesis of Antimony-Germanate-Silicate Glass Modified by P<sub>2</sub>O<sub>5</sub>. *Materials* **2017**, *10*, 1059. [[CrossRef](#)]
31. Ortiz-Mosquera, J.F.; Nieto-Muñoz, A.M.; Rodrigues, A.C. Precursor Glass Stability, Microstructure and Ionic Conductivity of Glass-Ceramics from the Na<sub>1+x</sub>Al<sub>x</sub>Ge<sub>2-x</sub>(PO<sub>4</sub>)<sub>3</sub> NASICON Series. *J. Non Cryst. Solids* **2019**, *513*, 36–43. Available online: <https://reader.elsevier.com/reader/sd/pii/S0022309319301541?token=1172499F341EDFD317F1C30D4F565807A1EB9067E74C82D6DE929E0D920E77D59F198FB3A2A6B8E1A80AD0346EE66B7D&originRegion=eu-west-1&originCreation=20220502094405> (accessed on 2 May 2022). [[CrossRef](#)]
32. Šesták, J.; Simon, P. *Thermal Analysis of Micro, Nano- and Non-Crystalline Materials: Transformation, Crystallization, Kinetics and Thermodynamics*; Springer Science & Business Media: Berlin/Heidelberg, Germany, 2012; ISBN 978-90-481-3150-1.
33. Ragiń, T.; Baranowska, A.; Zmojda, J.; Kochanowicz, M.; Miluski, P.; Mazur, D. Effect of Alkali Content on Spectroscopic Properties of Er/Ag Co-Doped Antimony-Germanate Glasses. In *Proceedings of the Photonics Applications in Astronomy, Communications, Industry, and High-Energy Physics Experiments 2018, Wilga, Poland, 3–10 June 2018*; Romaniuk, R.S., Linczuk, M., Eds.; SPIE: Wilga, Poland, 2018; p. 16.
34. Pařlick, C.; Ahrens, B.; Henke, B.; Johnson, J.A.; Schweizer, S. Differential Scanning Calorimetry Investigations on Eu-Doped Fluorozirconate-Based Glass Ceramics. *J. Non Cryst. Solids* **2010**, *356*, 3085–3089. [[CrossRef](#)] [[PubMed](#)]
35. Gavrilović, T.; Periša, J.; Papan, J.; Vuković, K.; Smits, K.; Jovanović, D.J.; Dramićanin, M.D. Particle Size Effects on the Structure and Emission of Eu<sup>3+</sup>:LaPO<sub>4</sub> and EuPO<sub>4</sub> Phosphors. *J. Lumin.* **2018**, *195*, 420–429. [[CrossRef](#)]
36. None Available Materials Data on EuPO<sub>4</sub> by Materials Project. 2020. Available online: <https://materialsproject.org/materials/mp-3219/> (accessed on 1 May 2022).
37. Patra, P.; Annapurna, K. Transparent Tellurite Glass-Ceramics for Photonics Applications: A Comprehensive Review on Crystalline Phases and Crystallization Mechanisms. *Prog. Mater. Sci.* **2022**, *125*, 100890. [[CrossRef](#)]
38. Szczodra, A.; Mardoukhi, A.; Hokka, M.; Boetti, N.G.; Petit, L. Fluorine Losses in Er<sup>3+</sup> Oxyfluoride Phosphate Glasses and Glass-Ceramics. *J. Alloys Compd.* **2019**, *797*, 797–803. [[CrossRef](#)]
39. Zeng, L.; Zhou, J. Analyses of Electric Field-Induced Phase Transformation by Luminescence Study in Eu<sup>3+</sup>-Doped (Na, K)<sub>0.5</sub>Bi<sub>0.5</sub>TiO<sub>3</sub> Ceramics. *Materials* **2020**, *13*, 1347. [[CrossRef](#)] [[PubMed](#)]
40. Linganna, K.; Jayasankar, C.K. Optical Properties of Eu<sup>3+</sup> Ions in Phosphate Glasses. *Spectrochim. Acta Part A Mol. Biomol. Spectrosc.* **2012**, *97*, 788–797. [[CrossRef](#)] [[PubMed](#)]
41. Pietrzak, T.K.; Gołębiewska, A.; Płachta, J.; Jarczewski, M.; Ryl, J.; Wasiucioneck, M.; Garbarczyk, J.E. Photoluminescence of Partially Reduced Eu<sup>2+</sup>/Eu<sup>3+</sup> Active Centers in a NaF-Al<sub>2</sub>O<sub>3</sub>-P<sub>2</sub>O<sub>5</sub> Glassy Matrix with Tunable Smooth Spectra. *J. Lumin.* **2019**, *208*, 322–326. [[CrossRef](#)]

42. Gopinath, R.J.M.; Gopi, S.; Simon, S.M.; Saritha, A.C.; Biju, P.R.; Joseph, C.; Unnikrishnan, N.V. Spectroscopic Analysis of Eu<sup>3+</sup> doped Silica-Titania-Polydimethylsiloxane Hybrid ORMOSILs. *RSC Adv.* **2020**, *10*, 20057–20066. [[CrossRef](#)]
43. Pawlik, N.; Szpikowska-Sroka, B.; Goryczka, T.; Pisarska, J.; Pisarski, W.A. Structural and Photoluminescence Investigations of Tb<sup>3+</sup>/Eu<sup>3+</sup> Co-Doped Silicate Sol-Gel Glass-Ceramics Containing CaF<sub>2</sub> Nanocrystals. *Materials* **2021**, *14*, 754. [[CrossRef](#)]